Analysis of Fluorophore Diffusion by Continuous Distributions of Diffusion Coefficients: Application to Photobleaching Measurements of Multicomponent and Anomalous Diffusion

N. Periasamy and A. S. Verkman
Departments of Medicine and Physiology, Cardiovascular Research Institute, University of California, San Francisco, California 94143 USA

ABSTRACT Fluorescence recovery after photobleaching (FRAP) is widely used to measure fluorophore diffusion in artificial solutions and cellular compartments. Two new strategies to analyze FRAP data were investigated theoretically and applied to complex systems with anomalous diffusion or multiple diffusing species: 1) continuous distributions of diffusion coefficients, $\alpha(D)$, and 2) time-dependent diffusion coefficients, $D(t)$. A regression procedure utilizing the maximum entropy method was developed to resolve $\alpha(D)$ from fluorescence recovery curves, $F(t)$. The recovery of multi-component $\alpha(D)$ from simulated $F(t)$ with random noise was demonstrated and limitations of the method were defined. Single narrow Gaussian $\alpha(D)$ were recovered for FRAP measurements of thin films of fluorescein and size-fractionated FITC-dextrans and Ficolls, and multi-component $\alpha(D)$ were recovered for defined fluorophore mixtures. Single Gaussian $\alpha(D)$ were also recovered for solute diffusion in viscous media containing high dextran concentrations. To identify anomalous diffusion from FRAP data, a theory was developed to compute $F(t)$ and $\alpha(D)$ for anomalous diffusion models defined by arbitrary nonlinear mean-squared displacement $\langle x^2 \rangle$ versus time relations. Several characteristic $\alpha(D)$ profiles for anomalous diffusion were found, including broad $\alpha(D)$ for subdiffusion, and $\alpha(D)$ with negative amplitudes for superdiffusion. A method to deduce apparent $D(t)$ from $F(t)$ was also developed and shown to provide useful complementary information to $\alpha(D)$. $\alpha(D)$ and $D(t)$ were determined from photobleaching measurements of systems with apparent anomalous subdiffusion (nonuniform solution layer) and superdiffusion (moving fluid layer). The results establish a practical strategy to characterize complex diffusive phenomena from photobleaching recovery measurements.

INTRODUCTION

Fluorescence recovery after photobleaching (FRAP) has been used extensively to study fluorophore diffusion in artificial solutions containing solutes and polymers, and in cellular membrane and aqueous compartments. In spot photobleaching, fluorophores in a defined volume are irreversibly bleached by a brief intense laser beam; the subsequent kinetics of fluorescence recovery in the bleached region provides a quantitative measure of fluorophore translational diffusion. For spot photobleaching in two dimensions (as in lipid membranes), computational methods have been reported to deduce fluorophore diffusion coefficient (D) from bleach spot profile and fluorescence recovery curve shape, $F(t)$ (Axelrod et al., 1976; Barisas and Leuther, 1979; Yguerabide et al., 1982; Van Zoelen et al., 1983; Soumpasis, 1983). However, it is often invalid to apply exact theories to determine D because of nonidealities in laser beam profile, fluorophore diffusion during the bleach time, and other complexities such as noncylindrical beam z-profile in three-dimensional aqueous compartments. For quantitative determination of fluorophore D in the aqueous phase of cell cytoplasm, we introduced a calibration procedure where the half-time ($t_{1/2}$) for fluorescence recovery in cells is compared to $t_{1/2}$ measured in thin layers of fluorophores dissolved in artificial solutions of known viscosity (Kao et al., 1993; Seksek et al., 1997). These analytical and empirical methods are useful for determination of single, time-independent diffusion coefficients, but are not easily adapted to complex diffusive phenomena such as anomalous diffusion or diffusion of multiple species with different diffusion coefficients.

Solute diffusion is described as "normal" or "simple" in a homogeneous medium such as a liquid solvent, in which case solute transport is described adequately by a single diffusion coefficient. There are many environments and situations in which solute diffusion cannot be described in terms of a single diffusion coefficient. One example is anomalous diffusion. The diffusion of a solute is said to be anomalous if the mean-squared displacement ($\langle x^2 \rangle$, see Theory section) varies with time in a nonlinear manner. In such systems the diffusion coefficient is not constant, but time- and/or space-dependent. A number of different physical mechanisms giving anomalous diffusion have been described (Bouchaud and Georges, 1990; Drake and Klafter, 1990; Klafter et al., 1996; Artuso, 1997) (see Discussion). Saxton has addressed several potential mechanisms of anomalous diffusion that are relevant to solute transport in cell membranes involving binding and collisional interactions with mobile and immobile obstacles (Saxton, 1990,

Received for publication 29 January 1998 and in final form 2 April 1998.

Address reprint requests to Alan S. Verkman, M.D., Ph.D., Cardiovascular Research Institute, 1246 Health Sciences East Tower, Box 0521, University of California, San Francisco, San Francisco, CA 94143-0521. Tel.: 415-476-8530; Fax: 415-665-3847; E-mail: verkman@itsa.ucsf.edu.

N. Periasamy's permanent address is Tata Institute of Fundamental Research, Mumbai, India.

0006-3495/98/07/557/11 $2.00

1993, 1994a, b, 1996). Another example of nonsimple diffusion is the presence of two or more diffusing species, each of which is described by a single diffusion coefficient. Without prior knowledge of the presence of multiple diffusing species, as is the case in cellular environments where heterogeneous binding can occur, the data can be wrongly interpreted as anomalous diffusion. Recently, anomalous diffusion of fluorophores in planar membranes and polymer networks has been found (Feder et al., 1996; Schutz et al., 1997; Starchev et al., 1997).

Photobleaching data in cell membrane and aqueous compartments have generally been analyzed in terms of a single diffusing component with or without an immobile fraction. In one study the possibility of two distinct diffusing species was considered (Gordon et al., 1995). The potential pitfalls in the assumption of simple diffusion and the significance of long tail kinetics in diffusive phenomena have been recognized (Nagle, 1992), and recent papers have begun to consider how to interpret photobleaching data in systems with complex or anomalous diffusion (Feder et al., 1996; Coelho et al., 1997; Ölveczky and Verkman, 1998). In this study we introduce the idea that fluorescence recovery data, $F(t)$, can be resolved in terms of a continuous distribution of diffusion coefficients, $\alpha(D)$. An effective regression method to recover $\alpha(D)$ from $F(t)$ was developed, validated, and applied to experimental photobleaching measurements on defined fluorophore mixtures. $\alpha(D)$ curve shape was then related to specific models of anomalous diffusion, and experimental examples are presented of anomalous subdiffusion and superdiffusion. An independent method to analyze $F(t)$ for anomalous diffusive processes in terms of time-dependent diffusion coefficients, $D(t)$, was also developed and validated experimentally. The results indicate that determination of $\alpha(D)$ and $D(t)$ from photobleaching data provides a systematic approach to identify and quantify simple and anomalous diffusive phenomena.

THEORY

Multicomponent and anomalous diffusion

Solute diffusion is described by the Smoluchowski equation,

$$\partial C(\mathbf{r}, t)/\partial t = D\nabla^2 C(\mathbf{r}, t) \quad (1)$$

where D is the diffusion coefficient, $C(\mathbf{r}, t)$ is the space- and time-dependent solute concentration, and ∇^2 is the Laplacian operator. The time course of fluorescence recovery after photobleaching, $F(t)$, is obtained by solving Eq. 1 with appropriate initial and boundary conditions. The general form of $F(t)$ for spot photobleaching (circle of radius w) in two dimensions is (Axelrod et al., 1976),

$$F(t) = f(K, t/\tau_D) \quad (2)$$

where K is the bleach depth and $\tau_D = w^2/4D$ is the "characteristic" diffusion time in two dimensions. Equation 2 is valid for FRAP experiments in planar membranes and in thin films of liquids. For fixed K and w, $F(t)$ is a function of $[Dt]$ so that the curve shape of $f(Dt)$ is identical for any fluorophore in any liquid. We define $f(Dt)$ as the *basis* recovery curve shape for simple diffusion of a single species (see below). A single parameter (for example, the recovery half-time, $t_{1/2}$) is thus sufficient to determine the diffusion coefficient of a single diffusing species. When there is more than one fluorophore in the sample, each with a different diffusion coefficient D_i, $F(t)$ becomes,

$$F(t) = \sum_i a_i f(D_i t) \quad (3)$$

where a_i is the fractional bleach depth of fluorophore i.

Anomalous diffusion of a solute is distinguished from simple (also called normal) diffusion by the time-dependence of the mean-squared displacement $\langle x^2 \rangle$ in single particle analysis. For simple diffusion in n dimensions, $\langle x^2 \rangle = 2nDt$. For anomalous diffusion $\langle x^2 \rangle$ does not increase linearly with time. The exact time-dependence of $\langle x^2 \rangle$ for anomalous diffusion depends on the physical structure (barriers, channels, etc.) of the medium in which the solute diffuses (see Discussion). Various mathematical forms for $\langle x^2 \rangle$ have been described, such as $\langle x^2 \rangle \sim t^\alpha$, where $\alpha \neq 1$ (Bouchaud and Georges, 1988). Anomalous diffusion is classified as subdiffusive ($\alpha < 1$), superdiffusive ($\alpha > 1$), or transiently anomalous ($\alpha \neq 1$ for $t_1 < t < t_2$). $\langle x^2 \rangle$ can in general be written,

$$\langle x^2 \rangle = 4tD(t) = 4tD_o g(t/\tau) \quad (4)$$

where D_o is a constant (unit cm^2/s), and τ is a characteristic time constant for anomalous diffusion (to make t/τ dimensionless). If Eq. 1 is valid for an anomalous diffusive process with D replaced by $D(t)$ (see below for a case when this is not true), then time can be parametrized in ζ,

$$\partial C/\partial \zeta = D_o \nabla^2 C;\ \zeta = \int g(t/\tau)dt \quad (5)$$

The spatial concentration profile of the solute obtained in anomalous diffusion at scaled time ζ is thus identical to that obtained for simple diffusion at time t. In the context of photobleaching experiments, the scaled variable $[D_o\zeta]$ corresponds to $[Dt]$ for simple diffusion. Thus, the fluorescence recovery curve shape is $f(Dt)$ for simple diffusion (see Eq. 2) and $f(D_o\zeta)$ for anomalous diffusion.

One example of anomalous superdiffusion is simple diffusion coupled with directional solute transport, such as fluid flow with a velocity of v cm/s. The mean-squared displacement increases nonlinearly with time,

$$\langle x^2 \rangle = 4Dt + v^2t^2 \quad (6)$$

The time-dependent diffusion coefficient in this case is $D(t) = D_o(1 + v^2t/4D)$. However, Eq. 1 is no longer valid unless an additional transport term is included (Axelrod et al., 1976). In this case the fluorescence recovery curve shape cannot be rigorously determined by time-scaling the

recovery curve shape $f(Dt)$ obtained in the absence of transport.

Strategies for analysis of *F*(*t*)

Two independent formalisms are described for the analysis of FRAP data in a model-independent manner. In the first case, experimental $F(t)$ is fitted to a continuous distribution of diffusion coefficients, $\alpha(D)$. For multiple diffusing species each undergoing simple diffusion, $\alpha(D)$ rigorously describes the contribution of each species to the recovery. As demonstrated in Results, $\alpha(D)$ is also useful for identification of anomalous subdiffusive and superdiffusive processes. In the second case, $F(t)$ is directly converted to $D(t)$. As shown in Results, $D(t)$ is useful for identification of simple and complex diffusive phenomena. For simple diffusion $D(t)$ is constant; for anomalous diffusion of a single diffusing species, $D(t)$ formally defines the diffusive process and can permit computation of $\langle x^2 \rangle$ versus time.

COMPUTATIONS

Distribution of diffusion coefficients

Fluorophore diffusion is described by a distribution of diffusion coefficients, $\alpha(D)$,

$$F(t) = \int \alpha(D) f(Dt) dD \tag{7}$$

where $f(Dt)$ is the basis function defined above. The maximum entropy method (MEM) is used here for determination of $\alpha(D)$ from $F(t)$. Explained briefly, let $\alpha(D)$ be the continuous distribution function with D in the range of D_{min} to D_{max} (typically 10^{-9} to 10^{-4} cm^2/s here). For numerical computation, $\alpha(D)$ is discretized at equal intervals in log(D) space,

$$F(t) = \sum_{i=1}^{m} \alpha_i f(D_i t) \tag{8}$$

where m is the number of discrete components, and α_i is the amplitude corresponding to the ith diffusion coefficient D_i. The MEM analysis gives a distribution $\alpha(D)$ that minimizes χ^2 and maximizes entropy S,

$$\chi^2 = \sum_i r_i^2 = \sum_i [F(t_i) - F_c(t_i)]^2/\sigma_i^2 \tag{9}$$

$$S = -\sum_i \alpha_i \log \alpha_i \tag{10}$$

where r_i is the residual, $F_c(t_i)$ the computed time course, and σ_i is the variance of the experimental data. Maximization of S assures that the distribution is as wide as allowed by the information content in the data (Swaminathan and Periasamy, 1996) so that a structured $\alpha(D)$ is obtained only if warranted by the data. The analysis of $F(t)$ begins by specifying an initial distribution for m (50 or 100) diffusion coefficients equally spaced in log(D) space. Without prior information about the distribution, a flat distribution of equal amplitude ($\alpha_i \sim 1/m$) is assumed. $F(t)$ is calculated using Eq. 8, followed by the calculation of r_i (for χ^2 computation) and appropriate partial derivatives (Skilling and Bryan, 1984). The distribution is modified using an m-dimensional correction vector generated to decrease χ^2 and increase S (Skilling and Bryan, 1984). An option to retain negative α_i values (or set them to zero) is exercised before the next iteration. The process is continued iteratively until the residuals are acceptably random or χ^2 does not decrease further. For each $F(t)$ the MEM analysis is repeated 10 times with different amplitudes for initial flat distributions to ensure robustness of the fitted $\alpha(D)$.

Applications of MEM to various types of experimental data, including biological systems, have been reviewed (Lavalette et al., 1991; Brochon, 1994). The MEM algorithm used here is similar to that described to obtain a distribution of lifetimes from fluorescence decay data (Swaminathan et al., 1994; Swaminathan and Periasamy, 1996). The basis function for lifetime analysis is an exponential $\exp(-t/\tau)$, whereas the basis function for analysis of FRAP data is $f(Dt)$.

Experimental determination of basis function *f*(*Dt*)

Fluorescein in PBS ($D = 2.6 \times 10^{-6}$ cm^2/s) was used for generation of the basis function $f(Dt)$. $F(t)$ (0–200 ms) with bleach depth ~20% was obtained as the average of 100 measurements using a sample of thickness 5 μm. The basis function was found to be independent of bleach depth for depth <30%, and independent of sample thickness for thickness <8 μm. $F(t)$ was empirically fitted to a triple exponential function and the resultant smooth curve was converted to basis function $f(Dt)$ by multiplying t by 2.6×10^{-6}.

D(*t*) computation

As described above, the basis function $f(y)$ for simple diffusion ($y = Dt$) is equivalent to that for anomalous diffusion with $y = D_o\zeta$. $D(t) = dy/dt$ was computed from experimental $F(t)$ as follows: a smooth curve representation of y was obtained by cubic spline interpolation using $F_c(t_i) = f(y_i)$, where $F_c(t_i)$ is the smooth fitted datum for experimental $F(t_i)$. $D(t_i) = (y_{i+1} - y_{i-1})/(t_{i+1} - t_{i-1})$ was then computed.

F(*t*) simulations

$F(t)$ for specified $\alpha(D)$ was computed using Eq. 8 with cubic spline interpolation as necessary. Random noise was added to each data point, $F(t_i) + qz_i$, where q is an amplitude factor related to signal-to-noise (S/N) ratio, and z_i is a

Gaussian-distributed random number with zero mean and unit variance (generated as described by Press et al., 1988).

EXPERIMENTAL METHODS

Fluorescence recovery after photobleaching

The FRAP apparatus for these studies was described in detail previously (Kao and Verkman, 1996; Seksek et al., 1997). The output of an argon ion laser (488 nm, Innova 70-4, Coherent Inc., Santa Clara, CA) was modulated by serial acousto-optic modulators (response time <2 μs) and directed onto the stage of an inverted epifluorescence microscope. The beam was reflected by a dichroic mirror (510 nm) onto the sample through an objective lens (Nikon 20× dry, numerical aperture 0.75). For most experiments, the laser beam power was set to 50–100 mW and the attenuation ratio (the ratio of bleach to probe beam intensity) was set to 5000–15000. Sample fluorescence was filtered by serial barrier (Schott glass OG515) and interference (530 $\pm$ 15 nm) filters and detected by a gated photomultiplier (9828A; Thorn EMI) whose gain was decreased transiently during the bleach period. Photomultiplier signals were amplified and digitized at 1 MHz using a 14-bit analog-to-digital converter. Beam modulation, photomultiplier gating, and data collection were software controlled. Signals were sampled before the bleach (generally 10^3 data points in 100 ms), then at high resolution (1 MHz sampling rate) over 10–100 ms, followed by low resolution (generally 10^4 points) over 0.1 to >10 s.

Sample preparation and photobleaching procedures

Specified microliter solution volumes were "sandwiched" between two glass coverslips to produce aqueous layers of uniform thickness ~ 5 μm. Doubly size-fractionated FITC-dextrans and Ficolls with narrow size distributions were prepared as described previously (Seksek et al., 1997). Aqueous samples consisted of fluorescein, FITC-dextrans, and FITC-Ficolls, individually or in combinations, in phosphate-buffered saline (PBS). In some experiments, up to 45% nonfluorescent dextran (40 kDa, Pharmacia) was added to the saline. In an experiment to simulate subdiffusion, a PBS solution of fluorescein of nonuniform thickness in triangular trough channel (interferometry calibration standard described in Farinas and Verkman, 1996) was photobleached. In an experiment to simulate superdiffusion, the microscope stage was translated linearly at specified velocity during the bleach and probe periods. In all experiments beam intensity and attenuation ratio were adjusted to produce $<30\%$ bleaching and to avoid photobleaching by the probe beam. Measurements were done at 23°C in a temperature-controlled darkroom. Generally, data from 5 to 20 individual FRAP experiments were averaged for each stored recovery curve, except for the experiment simulating superdiffusion where no averaging was done.

RESULTS

Fig. 1 shows fluorescence photobleaching recovery curves $F(t)$ for single fluorophores in PBS: fluorescein (*A*), two FITC-Ficoll size fractions (*B* and *C*), and 70 kDa FITC-dextran (*D*). Using the MEM fitting procedure, $\alpha(D)$ with single peaks were obtained at 2.7×10^{-6} cm^2/s (fluorescein), 3.5×10^{-7} cm^2/s (FITC-Ficoll, fractions 30–33), 8.7×10^{-8} cm^2/s (FITC-Ficoll, fractions 10–13), and 2.3×10^{-7} cm^2/s (FITC-dextran, 70 kD). The $\alpha(D)$ produced good fits to $F(t)$ (*smooth curves, top panels*) with random distributions of residuals, $\Delta F(t)$. The $\alpha(D)$ distributions had narrow width except those for the large FITC-Ficoll (frac-

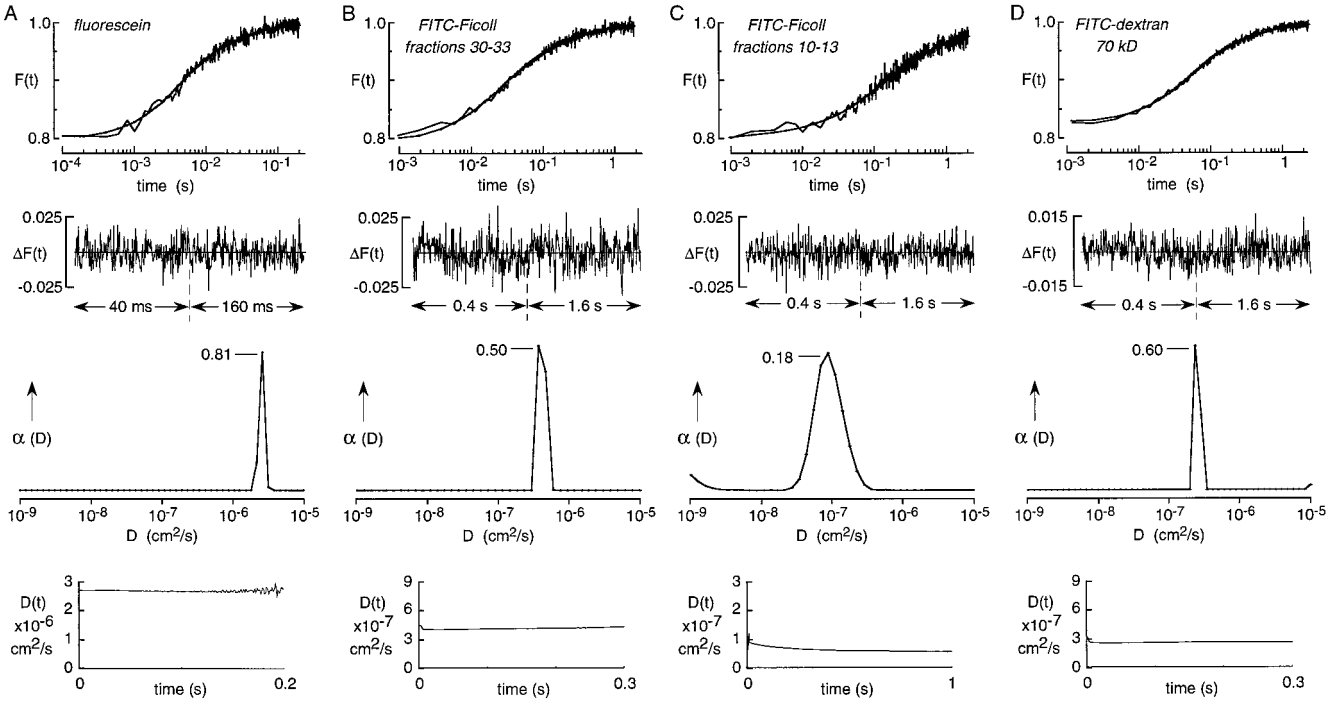

FIGURE 1 Fluorescence recovery data and fitted diffusion coefficient distributions for single fluorophores in PBS. (*A*) Fluorescein (50 μM), (*B*) FITC-Ficoll (fractions 30–33, 4 mg/ml), (*C*) FITC-Ficoll (fractions 10–13, 4 mg/ml), (*D*) FITC-dextran (70 kD, 4 mg/ml). *Top panels:* Experimental $F(t)$ data and fitted curve (*smooth line*) obtained by MEM analysis. *Second panels:* Residuals $\Delta F(t)$ of the fit. Residuals are shown on contiguous linear time scales as acquired experimentally (see Experimental Method). *Third panels:* Fitted distributions of diffusion coefficients $\alpha(D)$ by MEM analysis. *Bottom panels:* Time-dependent diffusion coefficient $D(t)$ determined from $F(t)$ (see Computations section).

tions 10–13). A narrow distribution indicates that the information content in the $F(t)$ data is excellent at the level of experimental noise (computed signal-to-noise ratio >40). The wider distribution for the large FITC-Ficoll is attributable to polydispersity in FITC-Ficoll size, and/or decreased data quality (see below). Computed $D(t)$ (*bottom panels*) were essentially constant in *A*, *B*, and *D*. The decreasing $D(t)$ in *C* is consistent with the possible polydispersity in FITC-Ficoll size mentioned above. These results establish the utility of the basis function approach, and indicate that recovery curve shape is invariant for simple diffusion of a single species.

Simulations of $F(t)$ were done to test the ability of the MEM analysis to recover $\alpha(D)$ distributions for nonsimple diffusion. Fig. 2 *A* shows five $\alpha(D)$: (*a*) single fluorophore undergoing simple diffusion; (*b*) two fluorophores with different diffusion coefficients, each undergoing simple diffusion; (*c*) Gaussian distribution; (*d*) asymmetric Gaussian distribution; (*e*) exponential distribution. Fig. 2 *B* shows simulated $F(t)$. The parameters for each $\alpha(D)$ (see Fig. 2 legend) were chosen to give identical recovery $t_{1/2}$ as seen by the common intersection point at $t_{1/2} = 40$ ms. The $F(t)$ curve shapes for the different $\alpha(D)$ distributions were qualitatively similar but had subtle quantitative differences. A magnified view of the differences in curve shape is provided in Fig. 2 *C*, showing the difference between each curve and curve *a*, $[F_x(t) - F_a(t)]$. The maximum deviation (0.005–0.015) of any curve from $F_a(t)$ is comparable in magnitude to the random noise [$\Delta F(t)$ in Fig. 1] in typical experimental photobleaching data.

MEM analysis was used to recover $\alpha(D)$ from $F(t)$. Gaussian random noise (0.005, S/N = 40) was added to the simulated $F(t)$ in Fig. 2 *B* to give S/N comparable to typical experimental data. Simulated $F(t)$ with this level of noise for the two-component system (case *b*) is shown in Fig. 3 *A* (*middle panel*). The $\alpha(D)$ distributions fitted to the $F(t)$ data with added noise are shown in Fig. 2 *D*, *a–e*. For one and two component systems, narrow, single and double-peaked distributions were recovered. The peak positions of $\alpha(D)$ are in good agreement with simulated parameters (see figure legend): $D = 3 \times 10^{-7}$ cm^2/s for single diffusion (*a*), and 1.0×10^{-7} and 9.7×10^{-7} cm^2/s for two-component diffusion (*b*). For Gaussian and skewed Gaussian simulations, the $\alpha(D)$ recovered by MEM analysis was broad and the shape of the distribution was similar to $\alpha(D)$ used for $F(t)$ simulation. The peak positions were close to those used for simulation: 4.3×10^{-7} cm^2/s (Gaussian, *c*) and 5.3×10^{-7} cm^2/s (skewed Gaussian, *D*). However, $\alpha(D)$ recovered for case *e* (peak at 5.3×10^{-7} cm^2/s) did not have the sharp rising edge of the exponential distribution. The results indicate limitations for quantitative recovery of $\alpha(D)$ that result from one or more of the following causes: poor signal-to-noise ratio, incomplete or truncated recovery curve, and insufficient or poor discretization of log(D) space.

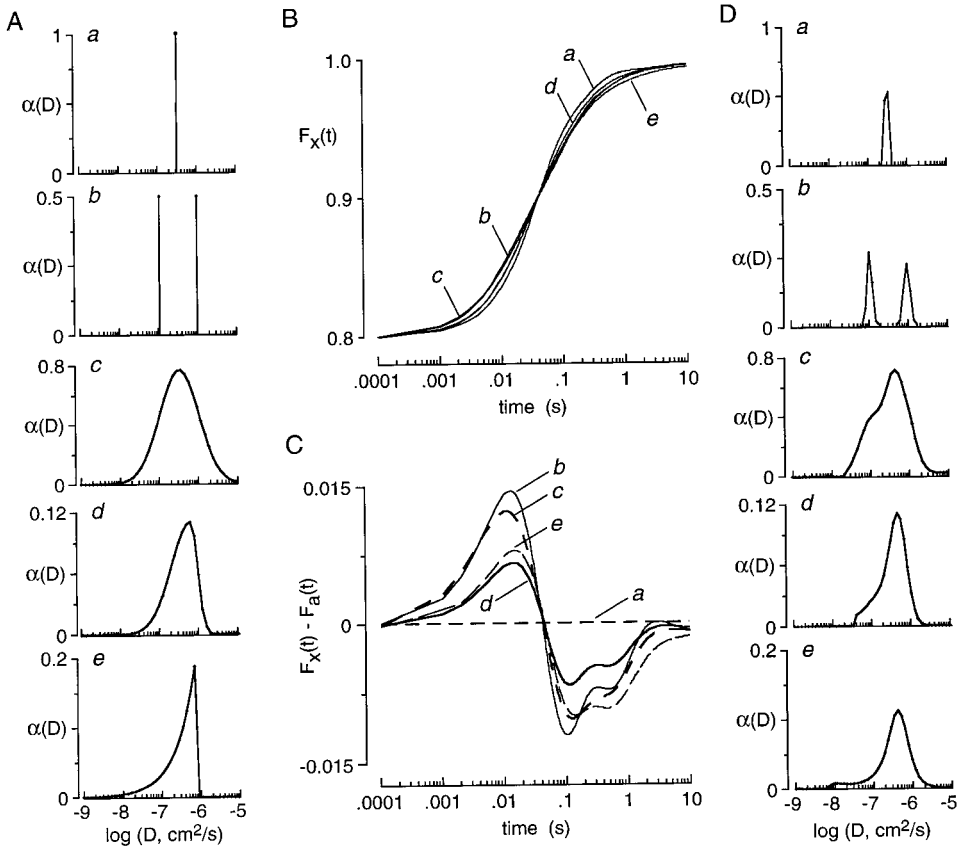

FIGURE 2 Simulated $F(t)$ and fitted $\alpha(D)$ for five diffusion coefficient distributions. (*A*) The five distributions (*a–e*) used for the $F(t)$ simulation are shown: (*a*) single diffusion coefficient, $D = 3.2 \times 10^{-7}$ cm^2/s; (*b*) two diffusion coefficients, $D_1 = 10^{-6}$ cm^2/s and $D_2 = 1.1 \times 10^{-7}$ cm^2/s with fractional amplitudes 0.5; (*c*) Gaussian distribution, $D_{max} = 3.3 \times 10^{-7}$ cm^2/s and width = 0.5 in log(D) space; (*d*) skewed Gaussian distribution, $D_{max} = 5.9 \times 10^{-7}$ cm^2/s, and widths 0.5 (*left side*) and 0.1 (*right side*) units in log(D) space; (*e*) exponential distribution, $D_{max} = 7.2 \times 10^{-7}$ cm^2/s and "decay" constant 0.5 units in log(D) space. D values and distribution widths were chosen to give identical $t_{1/2}$ for fluorescence recovery of 40 ms. (*B*) $F(t)$ simulated for the distributions (shown without added random noise). (*C*) Difference between curve $F_a(t)$ (single diffusion coefficient) and each of the other curves $F_x(t)$ shown on an expanded scale. (*D*) Random noise (S/N = 40) were added to simulated $F(t)$ in *A* and $\alpha(D)$ determined by MEM analysis.

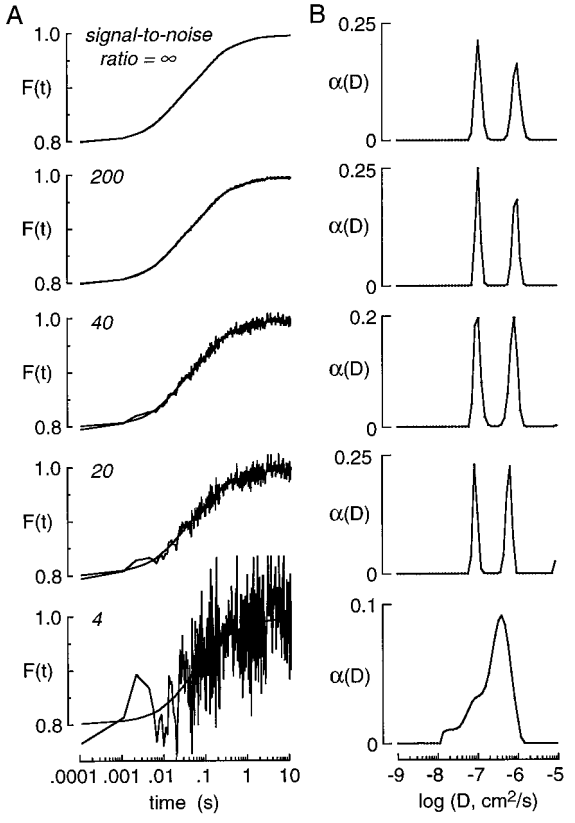

FIGURE 3 Resolution of diffusion coefficients in a two component system as a function of signal-to-noise ratio (S/N). (*A*) Simulated $F(t)$ for two diffusion coefficients (10^6 and 1.1×10^{-7} cm^2/s, fractional amplitudes 0.5) with added Gaussian random noise to give indicated S/N. (*B*) Fitted $\alpha(D)$ by MEM analysis.

The effect of signal-to-noise ratio in $F(t)$ was examined by the ability of MEM to resolve two diffusion coefficients ($D_1 = 10^{-6}$ and $D_2 = 1.1 \times 10^{-7}$ cm^2/s, fractional amplitudes 0.5). Fig. 3 *A* shows simulated $F(t)$ with added noise giving indicated S/N. Recovered $\alpha(D)$ are shown in Fig. 3 *B* with corresponding fitted $F(t)$ as the smooth curves in Fig. 3 *A*. Up to a noise level of S/N = 20, the two diffusing species could be resolved as narrow peaks in $\alpha(D)$. However, the accuracy of D value recovery was lessened with lowered S/N; in this example the position of one peak was shifted to lower D. The accuracy of the recovered diffusion coefficients was also tested in simulated $F(t)$ with S/N of 40 for different D_1/D_2 and fractional amplitudes. For fractional amplitudes of 0.5, a bimodal $\alpha(D)$ with two distinct diffusion coefficients could be obtained when D_1 and D_2 differed down to a factor of 3 (not shown). For $D_1/D_2 = 9$, two diffusion coefficients could be obtained when fractional amplitudes differed by up to a factor of 10. Where the $\alpha(D)$ fits were inadequate, unimodal broad distributions were recovered with peak positions located between the correct D values. Truncation of $F(t)$ tended to broaden $\alpha(D)$ distributions. For example, $F(t)$ in Fig. 3 *A* (curve *b*) was analyzed from zero time to times corresponding to $F(t) = 0.90-0.99$. Increasingly broad bimodal $\alpha(D)$ were obtained for 0.99–0.94, whereas unimodal broad $\alpha(D)$ were recovered with earlier truncation. Discretization of $\log(D)$ space also mildly affected $\alpha(D)$ width; empirically, use of 10–20 intervals in $\log(D)$ per decade was found to be optimal for the $F(t)$ curve fitting done in this study.

The MEM analysis was next tested on experimental $F(t)$ for two-component and three-component fluorophore mixtures consisting of combinations of fluorescein, FITC-Ficoll (fractions 30–33), and FITC-Ficoll (fractions 10–13) (see Fig. 1 for data on each individual component). For the two-component mixtures (Fig. 4, *A* and *B*), $\alpha(D)$ gave two peaks with D values (1.5×10^{-6} and 2.8×10^{-7} cm^2/s in *A*; 1.9×10^{-7} and 6.3×10^{-8} cm^2/s in *B*) in agreement to within a factor of 2 with those measured for the individual fluorophores (2.7×10^{-6} cm^2/s, Fig. 1 *A*; 3.5×10^{-7} cm^2/s, Fig. 1 *B*; 8.7×10^{-8} cm^2/s, Fig. 1 *C*). For the three-component system (Fig. 4 *C*), $\alpha(D)$ showed three peaks (1.8×10^{-6}, 1.9×10^{-7}, and 2×10^{-8} cm^2/s) in reasonable agreement with peak positions for the faster two of the three diffusing species. These results demonstrate the ability of MEM analysis to resolve the presence of multiple diffusing species, with typical accuracy for determination of individual D values to within a factor of 2.

Experimental $F(t)$ for fluorescein in complex heterogeneous media were obtained for analysis of $\alpha(D)$ and $D(t)$. The samples consisted of fluorescein in viscous dextran solutions (Fig. 5, *A* and *B*), fluorescein in a PBS layer of nonuniform thickness (trough channel simulating anomalous subdiffusion, Fig. 5 *C*) and fluorescein in a glycerol solution in which the solution layer was translated at constant velocity (simulating directed transport giving anomalous superdiffusion, Fig. 5 *D*). $\alpha(D)$ obtained by MEM analysis is shown for each case together with $D(t)$ computed from $F(t)$. In viscous dextran solutions (30 and 45% dextran with relative viscosities of ~6 and 30, respectively) $\alpha(D)$ was a narrow unimodal distribution and $D(t)$ is nearly constant, indicating simple diffusion. For photobleaching in the trough solution geometry, where fluorescence recovery requires diffusion from a thin to a thick region of the same, $\alpha(D)$ was broad and a peak at low D was seen, and $D(t)$ decreased with time. For anomalous superdiffusion in Fig. 5 *D*, $F(t)$ could not be fitted by MEM (*dashed curve in top panel*) with the constraint that all α_i are equal to or greater than zero, as was imposed in the previous analyses. However, $F(t)$ could be fitted reasonably well if the positive value constraint was omitted. The mathematical basis for negative α_i values in superdiffusion is described in the Discussion, where it is concluded that the need to include negative α_i is a useful signature for anomalous superdiffusion. $D(t)$ in Fig. 5 *D* increased with time, as expected for anomalous superdiffusion due to the moving liquid layer.

The results above indicate that simple diffusion can be confirmed by a single-peaked $\alpha(D)$ and constant $D(t)$. Other forms of $\alpha(D)$ and $D(t)$ indicate nonsimple diffusion. Simulations were done to show qualitative shapes of $\alpha(D)$ and $D(t)$ for several types of anomalous diffusion. In Fig. 6, $F(t)$ was simulated for diffusion models defined by the mean-

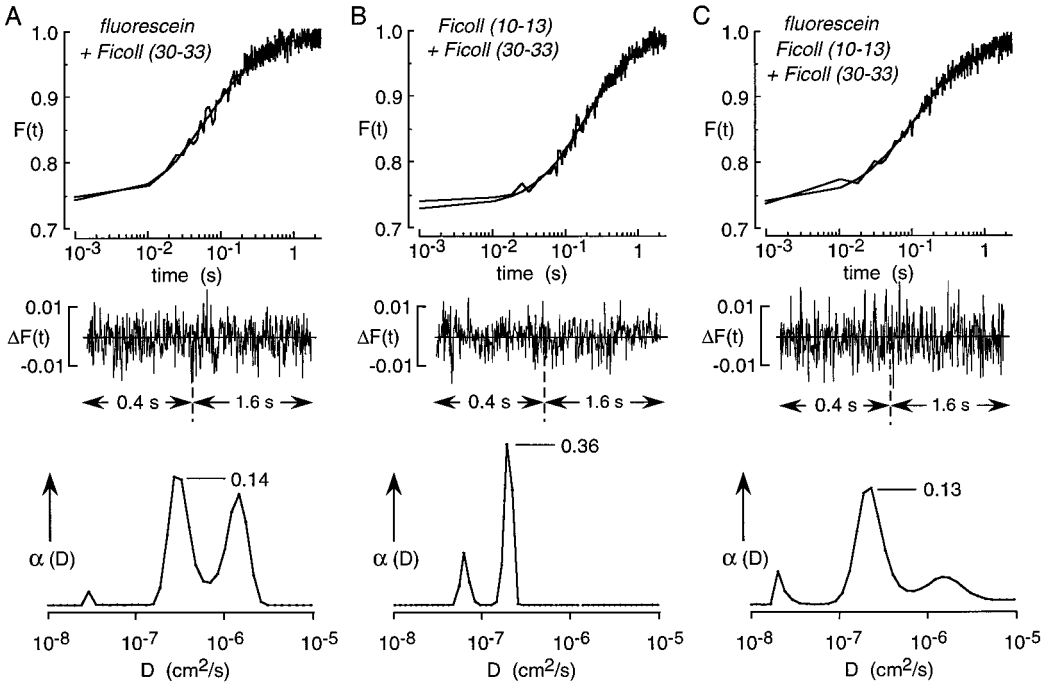

FIGURE 4 Resolution of multiple diffusing species for fluorophore mixtures in PBS. (*A*) Mixture of fluorescein and FITC-Ficoll (fractions 30–33). (*B*) FITC-Ficolls (fractions 10–13 and 30–33). (*C*) Mixture of fluorescein and FITC-Ficolls (fractions 10–13 and 30–33). Experimental $F(t)$ and the fitted curves shown in top panel, residuals $\Delta F(t)$ in middle panel, and fitted $\alpha(D)$ in bottom panel.

squared displacement $\langle x^2 \rangle$ versus time relations, $\langle x^2 \rangle = (a)\ 4Dt$ (simple diffusion); $(b)\ 4Dt[a + (1 - a)\exp(-t/\tau)]$ (anomalous subdiffusion type I); $(c)\ 4Dt^m$, $m < 1$ (anomalous subdiffusion, type II); $(d)\ 4Dt^m$, $m > 1$ (anomalous superdiffusion). Fig. 6 *A* shows $\langle x^2 \rangle$ versus time plots with the corresponding $D(t)$ shown in Fig. 6 *B* as D/D_o vs. $\log(t)$. After inclusion of typical experimental noise (S/N = 40) into $F(t)$ (Fig. 6 *C*), $\alpha(D)$ were determined by MEM analysis (Fig. 6 *D*). Compared to $\alpha(D)$ for simple diffusion of a single species (model *a*), which is a narrow Gaussian, $\alpha(D)$ for anomalous subdiffusion was either unimodal with broad and asymmetric distribution (model *b*) or multimodal (model *c*). For superdiffusion (model *d*), $F(t)$ could not be fitted with the constraint that all $\alpha_i > 0$. $\alpha(D)$ required inclusion of negative α_i (*d* in Fig. 6 *D*) (see Discussion).

DISCUSSION

The purpose of this study was to develop and evaluate procedures to analyze fluorescence photobleaching recovery experiments on systems having complex diffusive properties. This study was motivated by the substantial body of photobleaching data on cell membranes and cytoplasm indicating that diffusion in biological systems is not simple and cannot be adequately described by a single invariant diffusion coefficient. Fluorophore diffusion in biological systems is often complex because of binding interactions that may produce apparent heterogeneity in diffusion coefficients or physical constraints that produce anomalous diffusive phenomena such as percolation, convection, and sieving (Aon and Cortassa, 1994; Kopf et al., 1996; Licinio and Teixeira, 1997). As discussed in the Introduction, little attention has been given to the analysis of photobleaching recovery measurements in terms of complex diffusive phenomena. Although the task of deducing physical diffusion mechanisms from photobleaching data is in general not a rigorously solvable problem having a unique solution, we demonstrated that considerable insight into diffusion mechanisms can emerge from analysis of the full fluorescence recovery curve shape.

Based on the results here, practical guidelines are proposed for the acquisition and analysis of photobleaching experiments in complex systems. The ability to resolve complex diffusive processes requires data over extended times (generally >10–100 recovery half-times) with good signal-to-noise ratio (generally >20:1). High-quality basis recovery curves for an appropriate sample (with simple diffusion) should be acquired for every set of photobleaching experiments to match optical and other instrumental parameters. It is also useful to measure the recovery of a second fluorophore with simple diffusion to confirm the accuracy of the basis curve. Because of the sensitivity of the $\alpha(D)$ and $D(t)$ analyses to nonrandom deviations, systematic errors in data acquisition should be avoided such as bleaching by the probe beam and drift in probe intensity or optical alignment. Another potentially serious systematic artifact can be the presence of recovery processes that are unrelated to solute diffusion, such as reversible photobleaching resulting from triplet state population and recovery. Finally, the acquisition of multiple $F(t)$ data sets with appropriate bleach

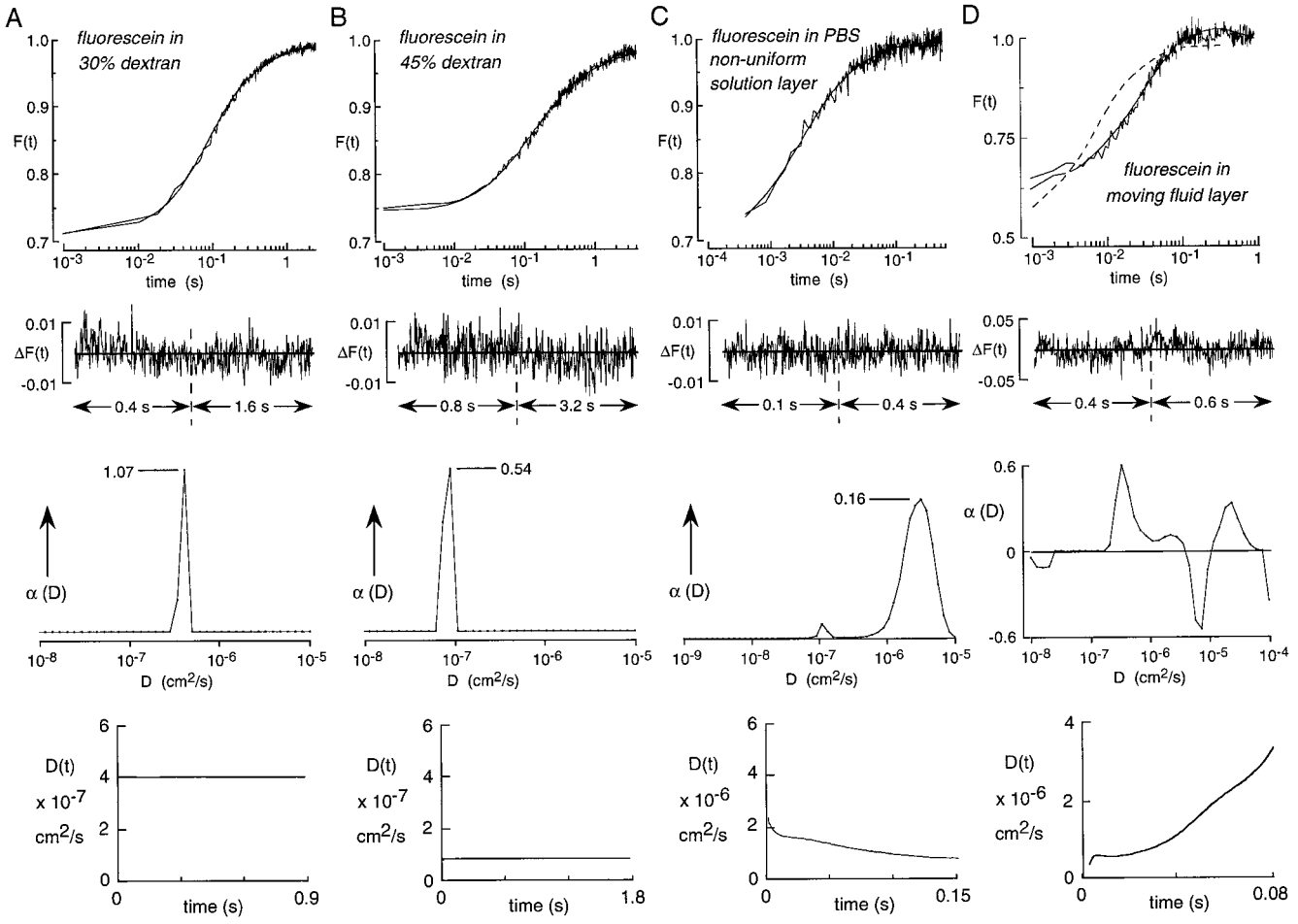

FIGURE 5 Photobleaching recoveries for fluorescein in different environments and analysis by $\alpha(D)$ and $D(t)$ methods. (*A* and *B*) Fluorescein (50 μM) in PBS containing indicated percentages of 40 kDa (nonfluorescent) dextran. (*C*) Fluorescein in PBS in a narrow triangular trough (simulating anomalous subdiffusion). A spot at the center of the trough was bleached where solution thickness was maximal. (*D*) Fluorescein in PBS containing 60% glycerol in which the microscope stage was linearly translated at velocity ~50 μm/s (simulating anomalous superdiffusion). The upper three panels show the experimental $F(t)$ and fitted curve, residuals $\Delta F(t)$ and fitted $\alpha(D)$. Single narrow peaks in $\alpha(D)$ with positive amplitudes were found for (*A*) and (*B*), and a broad peak with bimodal distribution for (*C*). For sample (*D*), $\alpha(D)$ regression required positive and negative amplitudes (see text). The bottommost panel shows fitted $D(t)$. $D(t)$ is approximately constant for (*A*) and (*B*), decreases for (*C*), and increases for (*D*).

depths (generally <30%) is indicated to test the robustness of the fitted results.

For the analysis of $F(t)$ curves, we propose that both the complementary distribution $\alpha(D)$ and time-dependent $D(t)$ analyses be carried out. It is recognized that $\alpha(D)$ formally describes the contributions of multiple diffusing species with differing D, and that $D(t)$ describes anomalous diffusion of a single diffusing species. However, there is generally little a priori knowledge about the nature of a complex diffusive process in a biological system. For example, the diffusion of a labeled membrane protein in the plane of a membrane might be affected by binding to other proteins or skeletal elements resulting in heterogeneity in diffusion coefficients; the complex membrane structure might produce anomalous subdiffusion, or energy-dependent transport or convective processes might produce anomalous superdiffusion. The complementary information afforded by determination of $\alpha(D)$ and $D(t)$ can be useful in defining the diffusion mechanism. A single narrow $\alpha(D)$ and constant $D(t)$ provides strong evidence for simple diffusion of a single species. The presence of a small number of distinct diffusing species produces narrow symmetric peaks in the $\alpha(D)$ analysis. Superdiffusion requires the inclusion of negative amplitudes in the $\alpha(D)$ analysis and produces an increase in diffusion coefficient over time. Anomalous subdiffusion produces a decrease in diffusion coefficient over time and a complex $\alpha(D)$ with positive amplitudes and broad peaks. There are likely to be cases that do not easily fit in the above categories where more than one complexity exists. Experimental maneuvers to distinguish among various possibilities are helpful in such situations, such as cellular energy depletion, use of different fluorophores, or biochemical modification of cell structure or metabolic status. In addition, single particle tracking could provide unique information about complexities and heterogeneity in $D(t)$ that cannot be deduced from ensemble-averaged pho-

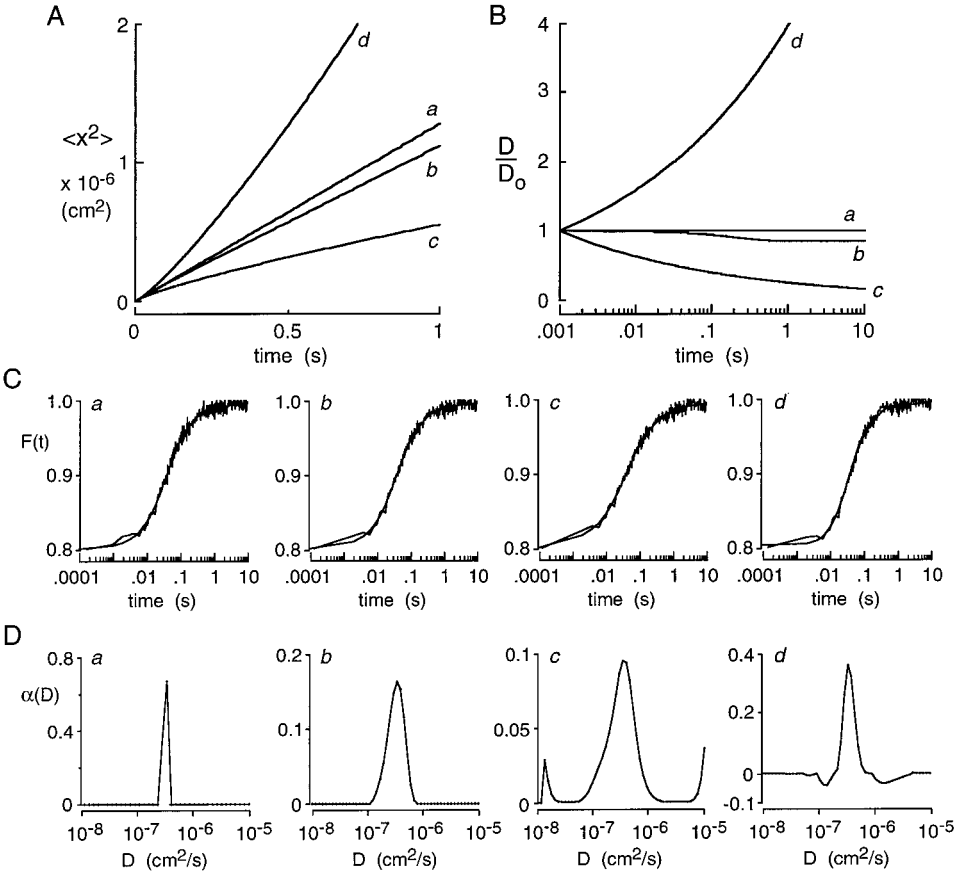

FIGURE 6 $F(t)$ and $\alpha(D)$ for simulated anomalous diffusion models. *Model a:* $D(t) = 3.2 \times 10^{-7}$ cm^2/s (simple diffusion); *model b:* $D(t) = 3.3 \times 10^{-7}$ [0.848 + 0.152 exp($-t$/0.2)] (anomalous subdiffusion, type I); *model c:* $D(t) = 2.17 \times 10^{-7}$ $(t/0.1)^{-0.2}$ (anomalous subdiffusion, type II); *model d:* $D(t) = 4.17 \times 10^{-7}$ $(t/0.1)^{0.2}$ (anomalous super diffusion). (*A*) mean-squared displacement (for single particle analysis) $\langle x^2 \rangle = 4tD(t)$ vs. t; curves *b*–*d* are nonlinear. (*B*) $D(t)$ plotted as D/D_o vs. t (D_o is the value of D at $t = 0.001$ s). (*C*) Simulated $F(t)$ with noise (S/N = 40) and smooth fitted curve obtained by MEM analysis. (*D*) $\alpha(D)$ determined by MEM analysis.

tobleaching measurements. Single particle tracking has been used in many studies of two-dimensional diffusion of bead-labeled, membrane-associated components (Qian et al., 1991; Feder et al., 1996; Saxton and Jacobson, 1997, and references therein); our laboratory developed an approach utilizing astigmatic optics to carry out single particle tracking in three dimensions (Kao and Verkman, 1994).

As discussed above, $\alpha(D)$ can be interpreted directly for multiple species with different diffusion coefficients undergoing simple diffusion. Although $\alpha(D)$ for anomalous diffusion cannot be simply interpreted in terms of heterogeneity in diffusive properties, there exists a mathematical rationale for its determination. In anomalous subdiffusion where $D(t)$ decreases monotonically with time, $F(t)$ is derived from basis function $f(Dt)$ by progressive time-stretching so that the second time derivative of $F(t)$ is negative at all times; therefore, a unique $\alpha(D)$ exists in which the α_i are positive. In anomalous superdiffusion where $D(t)$ increases with time, the inflection in $F(t)$ curvature produces both positive and negative $d^2F(t)/dt^2$. $\alpha(D)$ with only positive α_i cannot be fitted, but a unique $\alpha(D)$ with positive and negative amplitudes exists. Mathematically, if $f(Dt)$ is a single exponential function [1 − exp($-kt$)], then Eq. 7 formally defines $F(t)$ in terms of the Laplace transform of $\alpha(D)$; for experimental $F(t)$ with $dF(t)/dt > 0$, it is possible to write [1 − $F(t)$] as the ratio of two polynomials, which by the Heaviside theorem indicates the existence of a unique inverse Laplace transform (Pipes and Harvil, 1970). This argument is valid for arbitrary $f(Dt)$ that can be expanded as a sum of exponential functions. Our experience with many examples of simulated subdiffusion and superdiffusion (as in Fig. 6) supports the contention that an $\alpha(D)$ always exists with positive α_i for subdiffusion, and with positive and negative α_i for diffusion having a component of superdiffusion.

A key feature of the analysis procedures developed here was the use of a "basis function" $f(Dt)$ that describes the fluorescence recovery curve shape for simple diffusion of a single species. The basis function approach was validated by demonstrating accurate $\alpha(D)$ recovery for single and multi-component fluorophore mixtures. An experimentally derived basis function has important advantages over analytically derived recovery curves that require specification of laser beam profile and other details of the optics. The $f(Dt)$ used here is measured on "reference" samples under conditions identical to those used for the "test" samples. It is noted that the determination of accurate $f(Dt)$ is essential for the analysis. There are some restrictions on the use of an experimentally derived basis function. The basis function is formally defined in Eq. 2 for constant K, so that analysis of data with large bleach depths (generally >30%) should not be done using basis functions generated for small bleach depths. The requirement of identical beam geometry for reference and test samples generally restricts sample geometry to a thin layer, where beam width is constant. The basis

function determined for a thin fluid layer is then applicable for analysis of thin fluid layer test samples, which in cells would include plasma membranes, cytoplasm, and nucleoplasm. Analysis of photobleaching data in cellular organelles may require an analytical approach where the diffusion equation is solved directly (Partikian et al., 1998) or by a Monte Carlo computation (Ölveczky and Verkman, 1998) for specified organelle geometry.

The focus of the analysis here was on relating photobleaching recovery data to nonsimple diffusive phenomena as defined by $\alpha(D)$ and $D(t)$ functions. The specification of physical mechanisms that produce various forms of nonsimple diffusion is an important related issue that is not experimentally addressed in this study. The details of the physical structure of the environment in which a solute diffuses is the principal factor that determines the time and length scales in which the diffusion is simple versus anomalous. In pure liquids, diffusion of a solute is anomalous at extremely short and extremely long time and length scales (Chandrasekhar, 1943; Ovchinnikov et al., 1989; Bhattacharya and Bagchi, 1997). In liquids containing macromolecular solutes or other obstacles, solute diffusion may become nonsimple or anomalous in microseconds to minutes. Monte Carlo simulations of the diffusion of small solutes have been done as a function of the mobility and concentration of macromolecular obstacles (Saxton, 1990; 1994a). In the presence of immobile obstacles, a small solute diffuses through continuous aqueous channels surrounding the obstacles. When obstacle concentration exceeds the "percolation threshold" (C_p), continuous channels do not exist and diffusion becomes anomalous at all time and length scales. For $C < C_p$, solute diffusion is transiently anomalous at short times, in agreement with theoretical results based on percolation theory (Havlin and Ben-Avreham, 1987). According to percolation cluster theory, the dimensionality of the percolation channel is fractal when $C > C_p$; for $C < C_p$ the dimensionality is fractal for short length scale and normal at large length scale. If the obstacles are mobile, there is no percolation threshold at any obstacle concentration, but solute diffusion may be transiently anomalous.

Another important cause of anomalous diffusion in cell systems is binding of solutes to mobile and/or immobile obstacles. In a simple case, solute binding to a macromolecule is defined by a single equilibrium constant with a unique free energy of binding and mean residence time for the bound solute. In complex biological systems consisting of several types of macromolecules and binding sites, the binding energy and mean residence time may be quite heterogeneous. Solute diffusion under such conditions has been recognized to be important in biophysical phenomena (Nagle, 1992). Monte Carlo simulation of single particle diffusion for various binding models (obstruction/binding, distribution of binding/barrier energies) has revealed the interesting result that anomalous diffusion is sensitive to the initial condition of diffusing solute (Saxton, 1996).

The anomalous diffusion mechanisms referred to above are subdiffusive. Various physical mechanisms for anomalous superdiffusion have been discussed (Klafter et al., 1996, and references therein). Probability distributions with infinite variances (in contrast to finite variances in normal and anomalous subdiffusion) become important in nonlinear, fractal, chaotic, and turbulent systems. Such unusual probability distributions can produce so-called Levy flights and consequent anomalous superdiffusion. Superdiffusion of this kind has been observed experimentally in turbulent fluid flow (Solomon et al., 1993). Evidence for superdiffusion by the Levy flight mechanism has also been reported in a photobleaching study of the diffusion of dye bound to cylindrical micelles (Ott et al., 1990).

The physical mechanisms of nonsimple or anomalous diffusion discussed above are applicable to systems in thermal equilibrium where solute transport is mediated by random collisions. Living cells are thermodynamically open systems in which solutes and energy are continuously exchanged with the surroundings. Therefore, solute transport by mechanisms other than diffusion with random collisions is possible, such as directed transport of solutes (e.g., movement along microtubules) and fluid convection. Both processes can produce anomalous superdiffusion. Similarly, nonuniform distributions of solute or solvent can produce anomalous subdiffusion or superdiffusion, depending on the location of the bleach spot; the experimental examples of anomalous subdiffusion (Fig. 5 *C*) and superdiffusion (Fig. 5 *D*) belong to this category. The analysis methods introduced in this study should be particularly useful in photobleaching studies of living biological systems having one or more mechanisms of nonsimple diffusion.

We thank Drs. M. Dayel, O. Seksek, and R. Swaminathan for help with experimental photobleaching measurements, and Drs. J. Farinas, M. M. G. Krishna, and M. Saxton for helpful advice and discussions.

This work was supported by National Institutes of Health Grants DK43840 and DK35124, and National Institutes of Health Fogarty Research Award TW00704.

REFERENCES

Aon, M. A., and S. Cortassa. 1994. On the fractal nature of cytoplasm. *FEBS Lett.* 344:1–4.

Artuso, R. 1997. Anomalous diffusion in classical dynamical systems. *Phys. Rep.* 290:37–47.

Axelrod, D., D. E. Koppel, J. Schlessinger, E. Elson, and W. W. Webb. 1976. Mobility measurement by analysis of fluorescence photobleaching recovery kinetics. *Biophys. J.* 16:1055–1069.

Barisas, G., and M. D. Leuther. 1979. Fluorescence photobleaching recovery measurement of protein absolute diffusion coefficients. *Biophys. J.* 10:221–229.

Bhattacharya, S., and B. Bagchi. 1997. Anomalous diffusion of small particles in dense liquids. *J. Chem. Phys.* 106:1757–1763.

Bouchaud, J. P., and A. Georges. 1988. The physical mechanisms of anomalous diffusion. *In* Disorder and Mixing. E. Guyon, J. P. Nadal, and Y. Pomeau, editors. Kluwer Academic Publishers, Dordrecht, The Netherlands. 19–29.

Bouchaud, J. P., and A. Georges. 1990. Anomalous diffusion in disordered media—statistical mechanisms, models and physical applications. *Physics Rep.* 195:127–293.

Brochon, J. C. 1994. Maximum entropy method of data analysis in time-resolved spectroscopy. *Methods Enzymol.* 240:262–311.

Chandrasekhar, S. 1943. Stochastic problems in physics and astronomy. *Rev. Mod. Phys.* 15:1–89.

Coelho, F. P., W. L. C. Vaz, and E. Melo. 1997. Phase topology and percolation in two-compartment lipid bilayers: a Monte Carlo approach. *Biophys. J.* 72:1501–1511.

Drake, J. M., and J. Klafter. 1990. Dynamics of confined molecular systems. *Phys. Today*. 44:46–57.

Farinas, J., and A. S. Verkman. 1996. Measurement of cell volume and water permeability in epithelial cell layers by interferometry. *Biophys. J.* 71:3511–3522.

Feder, T. J., I. Brust-Mascher, J. P. Slattery, B. Baird, and W. W. Webb. 1996. Constrained diffusion or immobile fraction on cell surfaces: a new interpretation. *Biophys. J.* 70:2367–2373.

Gordon, G., B. Chazotte, X. F. Wang, and B. Herman. 1995. Analysis of simulated and experimental fluorescence recovery after photobleaching data for two diffusing components. *Biophys. J.* 68:766–778.

Havlin, S., and D. Ben-Avreham. 1987. Diffusion in disordered media. *Adv. Phys.* 36:695–798.

Kao, H. P., J. R. Abney, and A. S. Verkman. 1993. Determinants of the translational diffusion of a small solute in cytoplasm. *J. Cell Biol.* 120:175–184.

Kao, H. P., and A. S. Verkman. 1994. Tracking of single fluorescent particles in three dimensions: use of cylindrical optics to encode particle position. *Biophys. J.* 67:1291–1300.

Kao, H. P., and A. S. Verkman. 1996. Construction and performance of a photobleaching recovery apparatus with microsecond time resolution. *Biophys. Chem.* 59:203–210.

Klafter, J., M. F. Shlesinger, and G. Zumofen. 1996. Beyond Brownian motion. *Phys. Today*. 49:33–39.

Kopf, M., C. Corinth, O. Haferkamp, and T. F. Nonnenmacker. 1996. Anomalous diffusion of water in biological tissues. *Biophys. J.* 70: 2950–2958.

Lavalette, D., C. Tetreau, J. C. Brochon, and A. K. Livesey. 1991. Conformational fluctuations in protein reactivity. Determination of rate-constant spectrum and consequences in elementary biochemical processes. *Eur. J. Biochem.* 196:591–598.

Licinio, P., and A. V. Teixeira. 1997. Anomalous diffusion in ideal polymer networks. *Phys. Rev. E*. 56:631–634.

Nagle, J. F. 1992. Long tail kinetics in biophysics? *Biophys. J.* 63: 366–370.

Ölveczky, B. P., and A. S. Verkman. 1998. Monte Carlo analysis of obstructed diffusion in three dimensions: application to molecular diffusion in organelles. *Biophys. J.* 75:2722–2730.

Ott, A., J. P. Bouchaud, D. Langevin, and W. Urbach. 1990. Anomalous diffusion in living polymers—a genuine Levy flight. *Phys. Rev. Lett.* 65:2201–2204.

Ovchinnikov, A. A., S. F. Timashev, and A. A. Bely. 1989. Kinetics of Diffusion Controlled Chemical Processes. Nova Science Publishers, New York.

Partikian, A., B. Ölveczky, R. Swaminathan, Y. Li, and A. S. Verkman. 1998. Rapid diffusion of green fluorescent protein in the mitochondrial matrix. *J. Cell Biol.* 140:821–829.

Pipes, L. A., and L. R. Harvil. 1970. Applied Mathematics for Engineers and Physicists, 3rd ed. McGraw-Hill, New York. 161–172.

Press, W. H., S. A. Teulkolsky, W. T. Vetterling, and B. P. Flannery. 1988. Numerical Recipes in C. Cambridge University Press, New York.

Qian, H., M. P. Sheetz, and E. L. Elson. 1991. Single particle tracking: analysis of diffusion and flow in two-dimensional systems. *Biophys. J.* 60:910–921.

Saxton, M. J. 1990. Lateral diffusion in a mixture of mobile and immobile particles: a Monte Carlo study. *Biophys. J.* 58:1303–1306.

Saxton, M. J. 1993. Lateral diffusion in an archipelago. Dependence on tracer size. *Biophys. J.* 64:1053–1062.

Saxton, M. J. 1994a. Anomalous diffusion due to obstacles: a Monte Carlo study. *Biophys. J.* 66:394–401.

Saxton, M. J. 1994b. Single particle tracking: models of directed transport. *Biophys. J.* 67:2110–2119.

Saxton, M. J. 1996. Anomalous diffusion due to binding: a Monte Carlo study. *Biophys J.* 70:1250–1262.

Saxton, M. J., and K. Jacobson. 1997. Single particle tracking: applications to membrane dynamics. *Annu. Rev. Biophys. Biomol. Struct.* 26: 371–397.

Schutz, G. J., H. Schindler, and T. Schmidt. 1997. Single-molecule microscopy on model membranes reveals anomalous diffusion. *Biophys. J.* 73:1073–1080.

Seksek, O., J. Biwersi, and A. S. Verkman. 1997. Translational diffusion of macromolecule-size solutes in cytoplasm and nucleus. *J. Cell. Biol.* 138:131–142.

Skilling, J., and R. K. Bryan. 1984. Maximum entropy image reconstruction: general algorithm. *Mon. Not. R. Astron. Soc.* 211: 111–123.

Solomon, T., E. Weeks, and N. Swinney. 1993. Observation of anomalous diffusion and Levy flights in a 2-dimensional rotating flow. *Phys. Rev. Lett.* 71:3975–3978.

Soumpasis, D. M. 1983. Theoretical analysis of fluorescence photobleaching recovery experiments. *Biophys. J.* 41:95–97.

Starchev, K., J. Sturm, G. Weill, and C. H. Brogern. 1997. Brownian motion and electrophoretic transport in agarose gels studied by epifluorescence microscopy and single particle tracking analysis. *J. Phys. Chem.* 101:5659–5663.

Swaminathan, R., G. Krishnamoorthy, and N. Periasamy. 1994. Similarity of fluorescence lifetime distributions for single tryptophan proteins in the random coil state. *Biophys. J.* 67:2013–2023.

Swaminathan, R., and N. Periasamy. 1996. Analysis of fluorescence decay by the maximum entropy method: influence of noise and analysis parameters on the width of the distribution of lifetimes. *Proc. Ind. Acad. Sci. (Chem. Sci.).* 108:39–49.

Van Zoelen, E. J. J., G. J. Tertoolen, and S. W. de Laat. 1983. Simple computer method for evaluation of lateral diffusion coefficients from fluorescence photobleaching recovery kinetics. *Biophys. J.* 42:103–108.

Yguerabide, J., J. A. Schmidt, and E. E. Yguerabide. 1982. Lateral mobility in membranes detected by fluorescence recovery after photobleaching. *Biophys. J.* 39:69–75.